Modeling of deleterious phase precipitation during isothermal treatments in superduplex stainless steel

**J. M. Pardal · S. S. M. Tavares · M. P. Cindra Fonseca ·
J. A. de Souza · A. Loureiro · E. P. Moura**

Abstract The deleterious constituents σ, χ, and eutectoid γ_2 can precipitate during hot forming and welding operations in superduplex stainless steels. In this study the precipitation of these phases in superduplex UNS S32750 was investigated. Two materials with similar composition and quite different grain sizes were used in the study. Specimens were subjected to isothermal treatments in the 800–950 °C temperature range for time periods up to 240 min. Under these conditions, quantifications of deleterious phases by light optical microscopy were carried out in order to model the precipitation kinetics of these deleterious constituents. A sigmoidal equation, similar to the one developed by Johnson–Mehl–Avrami was fitted to all the analyzed temperatures. Precipitation velocity was evaluated so as to compare the kinetics of deleterious phases in the two materials. The activation energies for precipitation were calculated based on Arrhenius equation.

Introduction

Duplex stainless steel (DSS) and superduplex stainless steel (SDSS) have been widely employed in several sectors of industries due to their high mechanical resistance and pitting corrosion resistance. These characteristics are related to its dual phase microstructure, composed of similar quantities of austenite (γ) and ferrite (δ), and to the alloying elements Cr, Mo, and N [1].

However, during welding and forming operations, deleterious phase precipitation may compromise the use of these materials in the severe environmental conditions that they are exposed to. The main deleterious phases reported are sigma (σ), chi (χ), chromium nitrides, and carbides. χ is a Mo rich phase that is formed in the initial stages of aging in the 700–900 °C temperature range and is replaced by σ phase with the increase of the aging time [2]. σ phase is considered the most dangerous one due to its stability and harmful effects on toughness [3] and corrosion resistance [4]. Although σ can be formed by $\chi \rightarrow \sigma$ reaction, the main mechanism seems to be the eutectoid decomposition of ferrite by $\delta \rightarrow \sigma + \gamma_2$. Secondary austenite ($\gamma_2$) may be formed in this way, or precipitate independently from the ferrite phase. The growth of pre-existent γ islands during aging is also considered a kind of γ_2 formation. As its nitrogen and chromium content are lower than the parent austenite, generally γ_2 is reported to be deleterious due to its lower corrosion resistance [5].

The kinetics of precipitation of deleterious compounds is a function of the chemical composition of the material [6] and also the grain size [7]. The main objective of this article was to obtain a model for the kinetics of precipitation of the deleterious phases σ, χ, and γ_2 formed by eutectoid reaction in SDSS. Two SDSS with the same composition but quite different grain sizes were analyzed.

Moreover, a sigmoidal function was used in the modeling and activation energies for the precipitation were calculated using the Arrhenius equation. The results obtained are discussed on the basis of the differences between the grain sizes of the two SDSS studied.

J. M. Pardal · S. S. M. Tavares (✉) · M. P. Cindra Fonseca ·
J. A. de Souza · A. Loureiro
Departamento de Engenharia Mecânica, UFF–Universidade
Federal Fluminense, Rua Passo da Pátria, 156, Sala 302,
São Domingos, 24210-240 Niterói, RJ, Brazil
e-mail: ssmtavares@terra.com.br

E. P. Moura
Departamento de Engenharia Metalúrgica e Materiais,
UFC–Universidade Federal do Ceará, Fortaleza, CE, Brazil

Materials and methods

Two UNS S32750 SDSS with similar compositions and different grain sizes were analyzed. The fine-grained material was identified as SD-A and the coarser grained one as SD-B. The SD-A material was from a sheet with a thickness of 9.5 mm which was cold rolled and solution treated. SD-B specimens were from a bar with a diameter of 203 mm which was hot rolled and solution treated. This last procedure results in a much coarser grain size of ferrite and austenite phases. Table 1 presents the chemical composition of the materials analyzed.

Specimens with the dimensions of $15 \times 10 \times 5$ mm were taken from the materials in the as-received solution treated condition. Then, they were isothermally treated at 800, 850, 900, and 950 °C for 5, 15, 30, 45, 60, 90, 120, and 240 min intervals. After aging the specimens were cooled in water.

The metallographic analyzes were carried out in a NEOPHOT 32 light optical microscope (LOM), with the microstructures revealed by electrolytic etching in KOH solution. The quantifications of deleterious phases (χ, σ, and γ_2), were determined through *Image Tools v.3.0* [8] software, analyzing an average of 20 images per condition.

Some of the specimens that were heat treated and etched in KOH solution were characterized by SEM, using a JEOL model 6460LV. The ferrite and austenite grain size measurements were assessed by electron backscattered scanning diffraction (EBSD).

The modeling was carried out according to the following sigmoidal function:

$$f_{(t)} = f_s \cdot e^{-e^{(-n \cdot (t-K))}} \qquad (1)$$

where: $f_{(t)}$ volumetric fraction of the precipitated deleterious phase; f_s volumetric fraction of the precipitated deleterious phase saturated, to a certain temperature of heat treatment; n constant temperature dependent treatment related to the precipitation of the deleterious phase rate ($1/h$); t time of aging (h); and K time constant, dependent on the nucleation period and initial growth of the deleterious phase (h).

The linearization of the Eq. 1 allows for the obtaining of the constants n and K, as shown in Eq. 2.

$$\ln\left[-\ln\left(\frac{f_{(t)}}{f_s}\right)\right] = -n \cdot t + n \cdot K \qquad (2)$$

Constants n and K were determined for both steels and all the temperatures investigated by plotting $\ln(-\ln(f_{(t)}/f_s))$ versus t.

Deriving Eq. 1 in relation to time, an expression for the velocity of precipitation of deleterious phase can be obtained (3).

$$\frac{df_{(t)}}{dt} = \left(n \cdot e^{(-n \cdot (t-K))}\right) \cdot \left(f_s \cdot e^{-e^{(-n \cdot (t-K))}}\right) \qquad (3)$$

Results and discussions

Figure 1a, b show examples of EBSD phase map images which were used to determine the ferrite grain sizes in SDA and SDB materials, respectively. In these figures the austenite phase is black and ferrite grains are shown with different tonalities in the grayscale. The grains are distinguished by the tonality when the angular difference of orientation between them is greater than 15°. Considering this threshold value, the EBSD software calculates the average ferrite grain size. Using phase maps for austenite (not shown), the grain sizes of this phase for both materials could also be measured. Table 2 shows the ferrite and austenite percentages and average grain sizes measured by EBSD by analysis of 10 different fields in the SDA and SDB materials.

Figure 2a shows an example of image obtained by LOM which was used for deleterious phase quantification. The dark regions revealed by the electrolytic etching in KOH solution accounts for the deleterious phase precipitates (χ, σ, and γ_2). The original image of Fig. 2a is treated and converted into Fig. 2b, which is effectively analyzed with the aid of *Image Tools* free software [8]. The resolution between these three phases is only possible by SEM analysis, as shown in Fig. 3a–d for the specimens treated at 850 and 900 °C for 60 min, respectively.

Figure 4 shows the $\ln(-\ln(f_{(t)}/f_s))$ versus t curves for the SD-A and SD-B steel specimens that were heat treated at 900 °C. The n and K values obtained for SD-A were 3.56 and 0.16 with a correlation coefficient of $R^2 = 0.98$. For SD-B steel n and K were 4.71 and 0.41, respectively, with

Table 1 Chemical compositions of materials studied

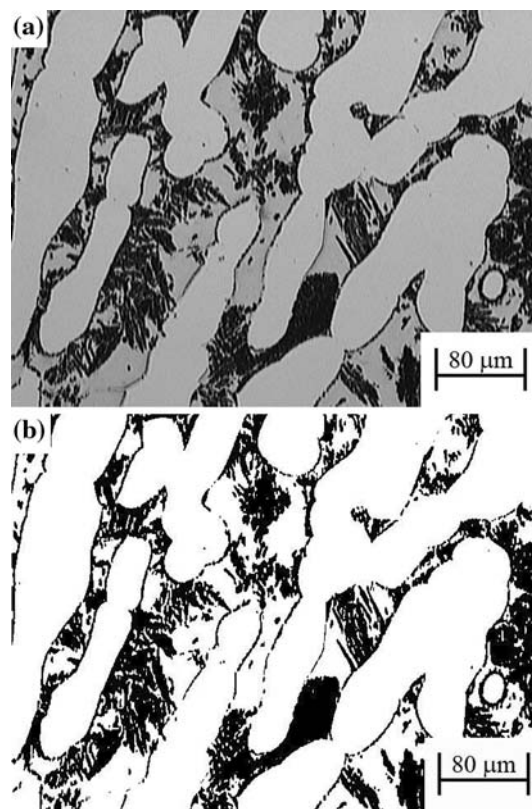| Material	Chemical composition (% weight). Fe balance.										
	Cr	Ni	Mo	Mn	Si	N	Cu	W	C	P	S
SD-A	24.57	6.68	3.75	0.83	0.34	0.28	0.25	–	0.02	0.03	0.000
SD-B	24.80	6.75	3.79	0.78	0.54	0.27	0.10	0.04	0.02	0.03	0.001
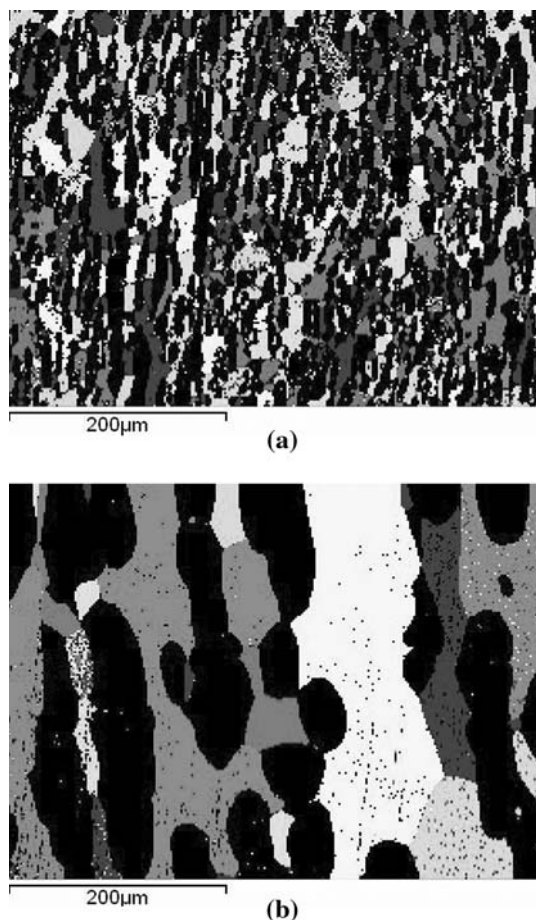
Fig. 1 EBSD images obtained for ferrite grain size measurement in the as received condition used for (a) SD-A; and (b) SD-B

Fig. 2 Example of deleterious phases quantification. (a) SD-B specimen treated at 850 °C for 60 min obtained by LOM. (b) Image treated and converted to binary pixels counted by *Image Tools* software

$R^2 = 0.99$. Figure 5 shows the plot of sigmoidal functions using the n and K values obtained. Three stages in the formation of deleterious phases can be highlighted:

- Stage I: period of nucleation and initial growth of deleterious phases.
- Stage II: interval of deleterious phase growth, in which the maximum velocity of precipitation is reached.
- Stage III: saturation of deleterious phase precipitation in the ferrite (δ).

The values of constants n and K obtained in all conditions are shown in Table 3. Correlation coefficients are also

shown and proved that the model is a good way of describing the precipitation behavior. Sigmoidal functions were also successfully used in the study of Cortie and Jackson in duplex steel [9].

Figure 6a–f shows the microstructural evolution of specimens treated at 800 °C. Figure 7 presents the curves correspondent to the volumetric fraction and the precipitation velocity of the deleterious phases of the materials analyzed at 800 °C. The maximum velocity for each condition is reached when the sigmoidal function crosses its inflexion point.

Analyzing the results of Fig. 7, it can be considered that the nucleation and growth period is significantly shorter in the fine-grained material (SD-A), corroborating with

**Table 2** Percentages of phases and grain size in materials SD-A and SD-B as received

Material	Ferrite (δ)			Austenite (γ)		
	Volumetric fraction	Grain size		Volumetric fraction	Grain size	
	(%)	(μm)	ASTM no.	(%)	(μm)	ASTM no.
SD-A	55.05	29.42	12.1	44.95	24.75	12.3
SD-B	49.95	132.36	9.9	50.05	138.32	9.9
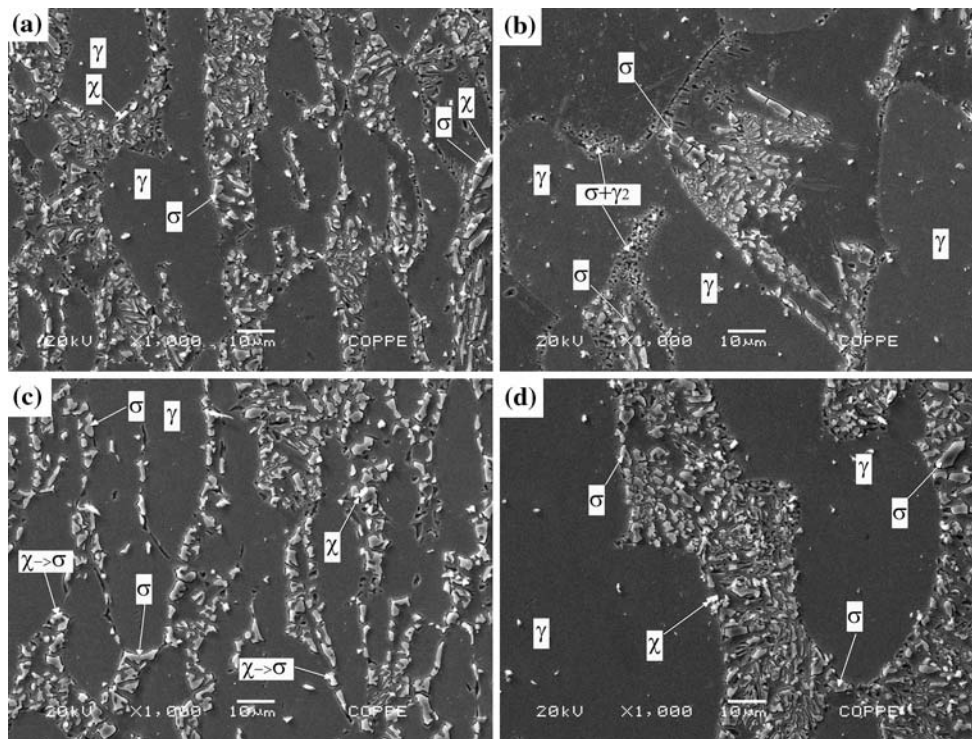
Fig. 3 Deleterious phases observed through SEM. (**a**) SD-A, (**b**) SD-B: treatments at 850 °C for 60 min. (**c**) SD-A, and (**d**) SD-B: treatments at 900 °C for 60 min
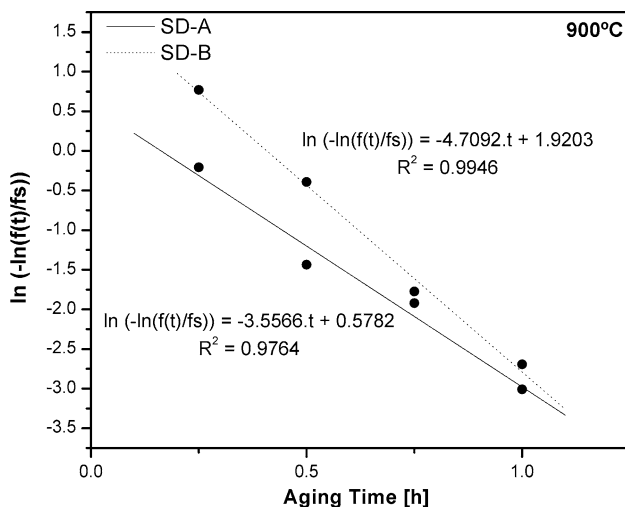
Fig. 4 Kinetics modeling of precipitation at 900 °C. Linear fitting to obtain n and K constants for SD-A and SD-B materials
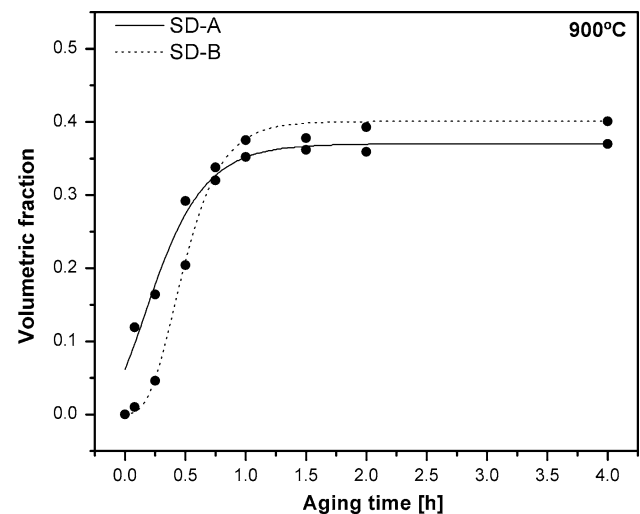
Fig. 5 Fitting of sigmoidal functions to model the precipitation kinetics at 900 °C. Curves of the volumetric fraction of SD-A and SD-B materials

results previously presented [7]. However, when stage II is reached, kinetics becomes more intense in the coarser grained SD-B steel. Some facts may contribute to this behavior:

– The Cr and Mo concentrations of ferrite phase in material SD-B must be relatively higher than in SD-A, because the compositions of both steels are very

similar, but SD-B contains less ferrite than SD-A in the initial condition. This contributes to the higher overall kinetics of deleterious phase precipitation in material SD-B, which is mathematically characterized by the higher n and maximum velocity values.

– On the other hand, nucleation is much faster in the fine grained SD-A material than in SD-B, which is correlated

**Table 3** n and K values obtained for all conditions of aging

Temperature (°C)	SD-A			SD-B		
	n	K	R^2	n	K	R^2
800	1.72	0.66	0.99	1.99	1.20	0.93
850	3.35	0.32	1.00	2.56	0.69	0.94
900	3.56	0.16	0.98	4.71	0.41	0.99
950	3.13	0.01	0.99	4.14	0.32	0.94

to the higher density of grain boundaries. Nucleation rate increases with the multiplication of nucleation sites.

– In stage III, SD-B reaches a higher saturation value than SD-A. Observing Fig. 8a, b the fine grained material (SD-A) shows many large γ_2 particles precipitated inside the ferrite domains, while the coarser grained material (SD-B) shows a higher proportion of deleterious phases
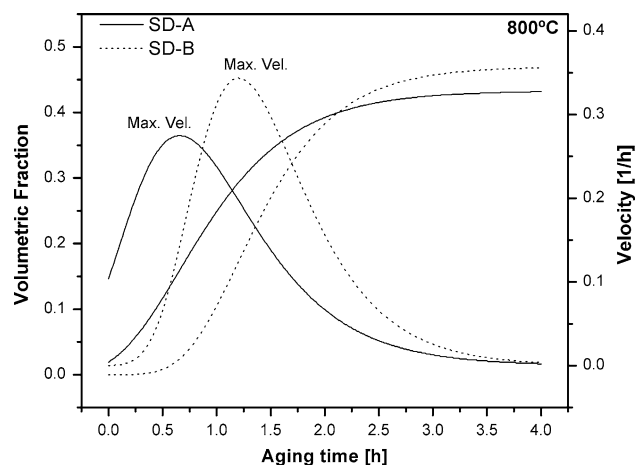
Fig. 7 Modeling of precipitation kinetics at 800 °C. Curves of volumetric fraction and velocity of deleterious phases precipitated for SD-A and SD-B
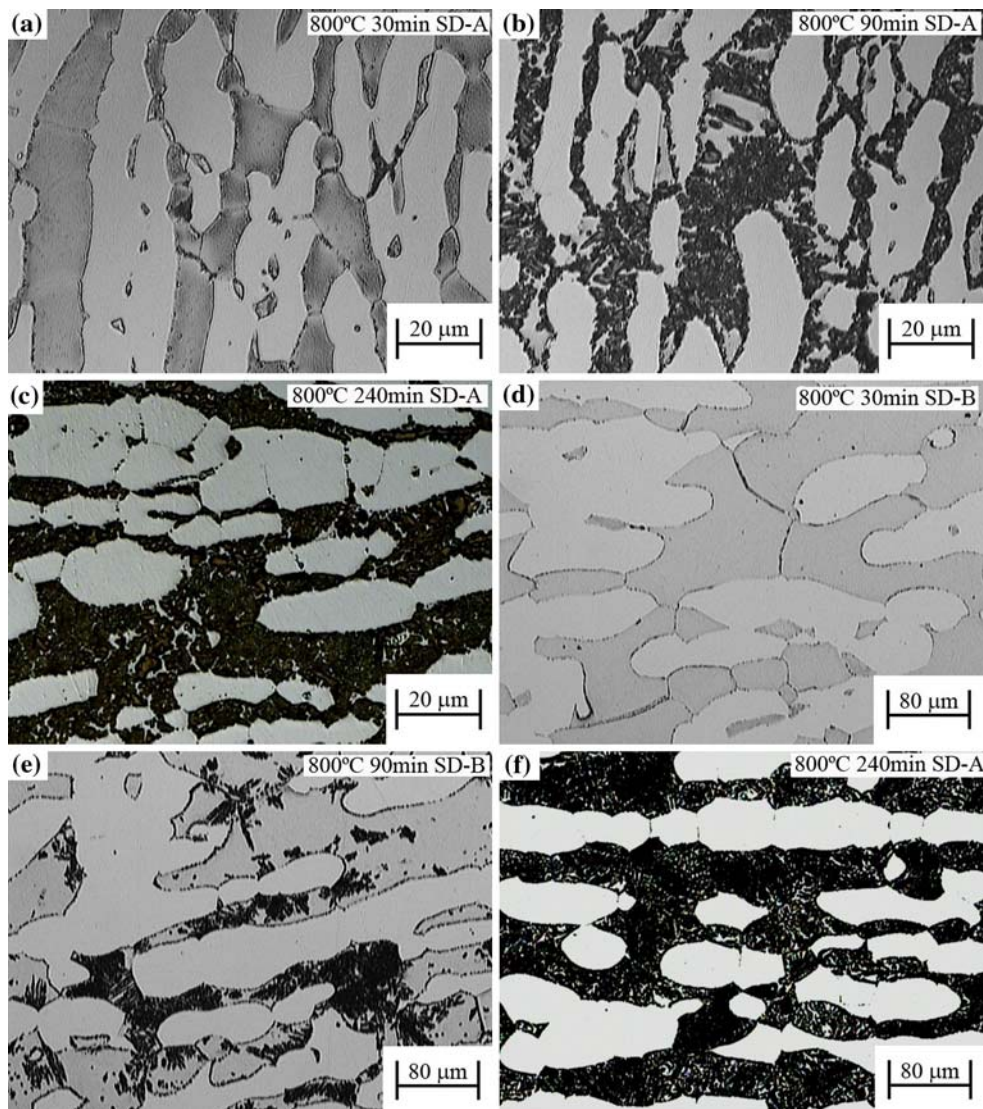
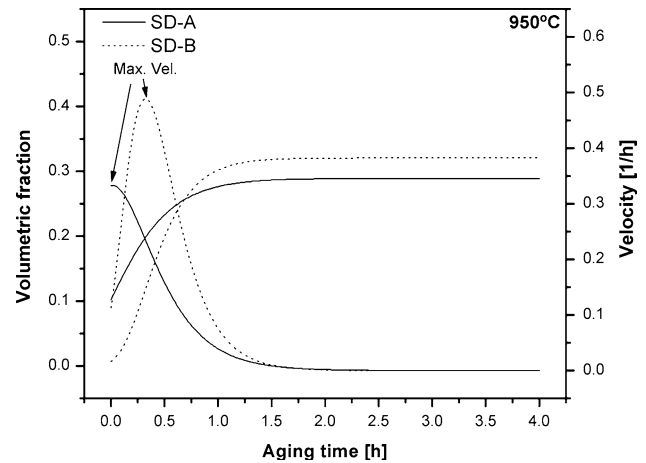**Fig. 6** Microstructural evolution of the deleterious phases precipitated at 800 °C for SD-A (**a–c**) and SD-B (**d–f**)
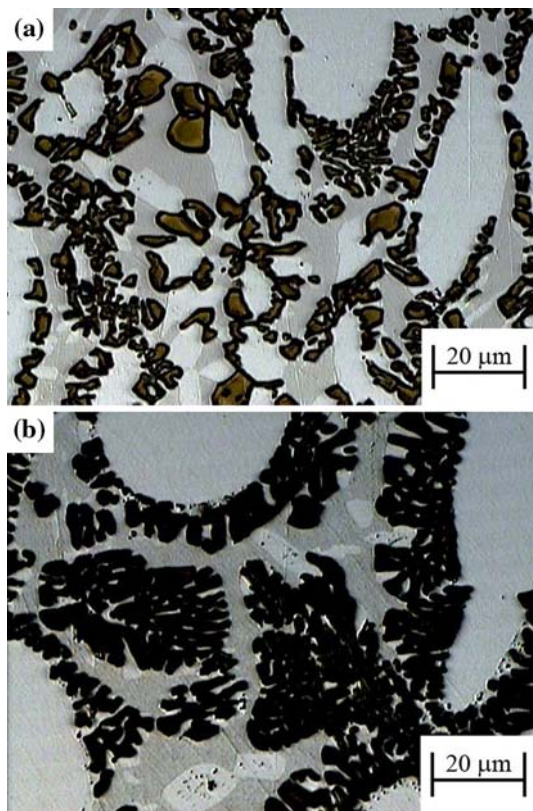
Fig. 8 Characterization, by LOM, of amount and size of deleterious phases precipitated at 950 °C for 120 min. (**a**) SD-A, and (**b**) SD-B

Fig. 9 Modeling of precipitation kinetics at 950 °C. Curves of volumetric fraction and velocity of deleterious phases precipitated for SD-A and SD-B

originated from the eutectoid decomposition of δ. The greater amount and larger size of independent γ_2 in material SD-A can be attributed to its higher grain boundary areas available to the $\delta \rightarrow \gamma_2$ transformation. Although the γ_2 particles precipitated at the ferrite grain boundaries can create Cr and Mo rich regions, as well as accelerate the formation of χ and σ in the initial stage, in a further step they act as barriers, creating an impingement effect. This explains the lower saturation values achieved in material SD-A. The less pronounced precipitation of independent γ_2 in SD-B contributes to the higher maximum velocity of precipitation in this material in stage II.

The curves obtained with specimens aged at 850 and 900 °C (not shown) have similar features as those observed in specimens aged at 800 °C, but with some differences. The increase of aging temperature reduces stages I and II and also decreases the volumetric fraction values achieved in stage III, for both materials. In all conditions the saturation value was higher in the SD-B material than in the SD-A material for the same the reasons that were explained in the previous paragraph for curves obtained at 800 °C.

Figure 9 shows the volumetric fraction and precipitation velocity of the deleterious phases obtained at 950 °C. At

this temperature, deleterious phase amounts at saturation are considerably lower than those observed at lower temperatures, which is a consequence of the more intense γ_2 precipitation. This microstructural feature can be observed by comparing the microstructures formed at 950 °C (Fig. 10a–f) to those found in specimens aged at 800 °C (Fig. 6a–f).

Figure 11 shows how the K constant value diminishes with the increase of aging temperature. In all temperatures, the fine grained condition (SD-A) has a nucleation and initial growth periods much lower than SD-B.

Figure 12 indicates the correlation between the n value obtained for each isothermal condition and the maximum precipitation velocity, correspondent to stage II. All conditions indicate that the velocity in stage II is higher in SD-B, except for aging at 850 °C.

The activation energy for the precipitation of the deleterious phases in SDSS can be obtained through the graphic representation of the logarithm of time correspondent to the maximum precipitation velocity versus $1/T$, i.e., the logaritmization of the Arrhenius equation:

$$\ln(t) = \frac{Q}{RT} + C \qquad (4)$$

where: Q activation energy for the precipitation of deleterious phases (kJ/mol); t time in which maximum precipitation velocity is achieved at each aging temperature (h); R universal constant of the gases (0.008314 kJ/mol K); C constant independent from temperature and T temperature of treatment (K).

Activation energies are calculated from the angular coefficients of the straight lines, as shown in Fig. 13. SD-A and SD-B present activation energies equal to 162.04 and 98.37 kJ/mol, respectively. Although stage I is more
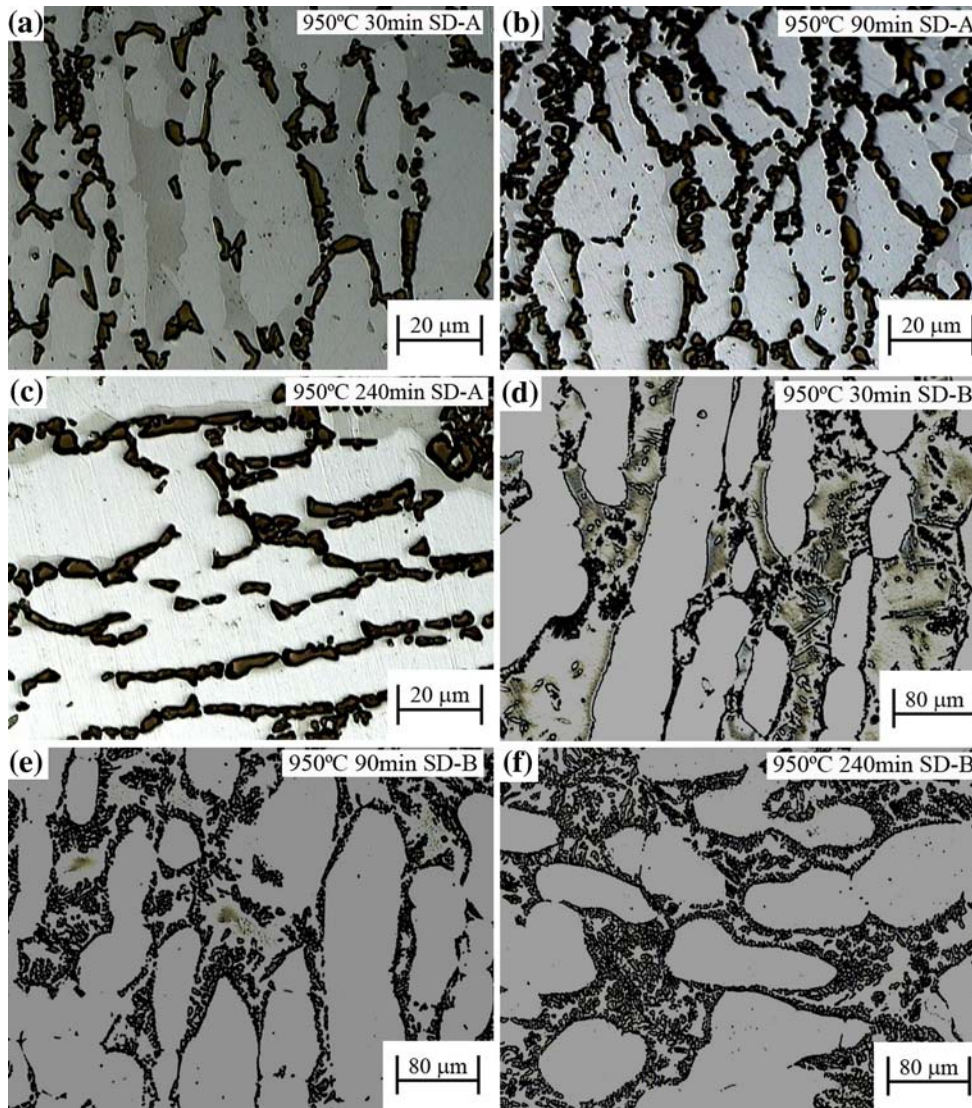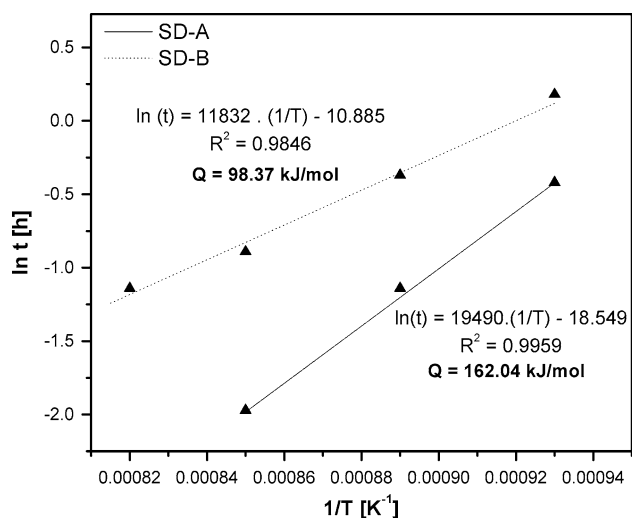
Fig. 10 Microstructural evolution of the deleterious phases precipitated at 950 °C for SD-A (**a–c**) and SD-B (**d–f**)
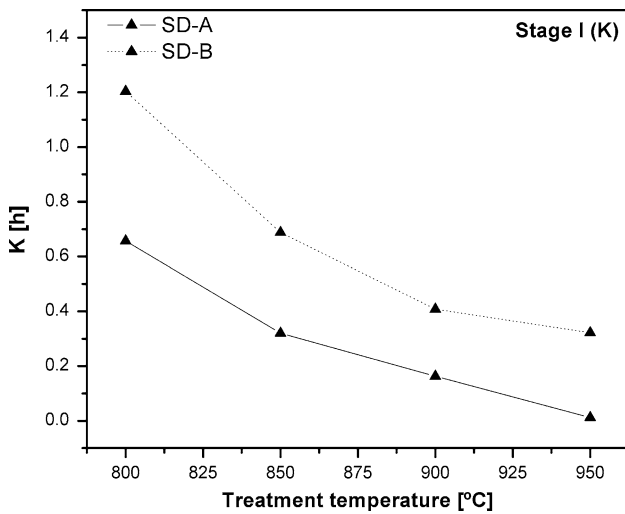
Fig. 11 *K* values in function of aging temperature
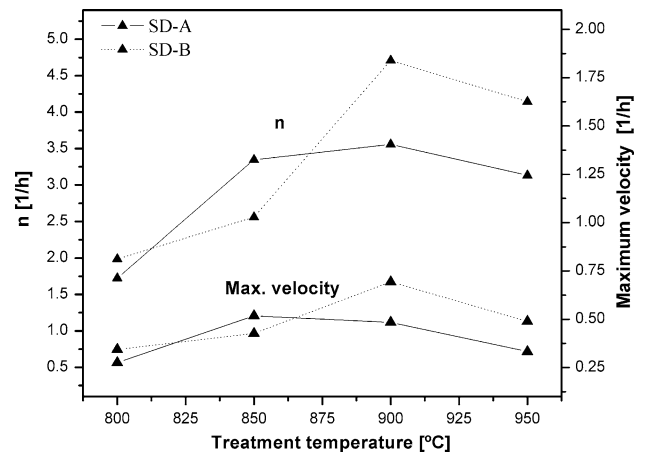
Fig. 12 Comparison between the *n* and the maximum velocity values in function of the aging temperature

Fig. 13 Determination of activation energy to the precipitation of deleterious phases in the SD-A and SD-B

prolonged in SD-B, the lower velocity and saturation values of the deleterious phases of SD-A determines a lower activation energy for this material. Such a factor may be attributed to the coarser plates of deleterious phase precipitation and large independent γ_2 plates, providing, in intermediary and final stages, a barrier to the deleterious phase precipitation. On the other hand, the higher concentration of elements, such as Cr and Mo, in the ferritic phase of SD-B also aids the transformation of this material.

Conclusions

Based on the results obtained in this study, it may be concluded that:

1. The kinetics of deleterious phases (χ, σ, and γ_2) precipitation in UNS S32750 superduplex steels with similar compositions and quite different grain sizes, during isothermal aging in the 800–950 °C temperature range, was modeled by sigmoidal functions. The velocity of precipitation was obtained by derivation of the phase amounts versus aging time curves.
2. Three different stages occurred in the evolution of the precipitated deleterious phases. Stage I: refers to the nucleation and growth of the initial deleterious phases. Stage II: relative to the growing interval of the precipitation of the deleterious phases. Stage III: the time interval taken for the saturation of the ferrite to be reached.
3. The period of nucleation and growth, characterized by the K constant, is lower in the fine grained SD-A material in all the treatment conditions.

4. The maximum velocity of precipitation is generally higher in the coarser grained SD-B material, except for specimens aged at 850 °C. In the model, the constant n is related to the value of the maximum velocity.
5. Large, independently precipitated γ_2 plays an important role in the precipitation process. Markedly, the higher amount of this γ_2 in the SD-A material acts as a barrier to $\delta \rightarrow \sigma$ and $\delta \rightarrow \gamma_2 + \sigma$ transformations. As a consequence, a lower saturation value and slower overall kinetics of precipitation is found in the fine-grained material in relation to the coarser grained one, despite of the more intense nucleation in the fine-grained steel.
6. High aging temperatures also induce the formation of thicker lamellar and coarse plates of σ, with γ_2 precipitated around them. At 950 °C the amounts of σ phase precipitated are much lower and the amounts of γ_2 much higher than at 800 °C.
7. Activation energies for precipitation were 162.04 and 98.37 KJ/mol for SD-A (fine-grained) and SD-B (coarse-grained), respectively.

References

1. Muthupandi V, Srinivasan PB, Seshadri SK, Sundaresan S (2003) Mater Sci Eng A A358:9
2. Chen TH, Weng KL, Yang JR (2002) Mater Sci Eng A A338:259
3. Tavares SSM, Da Silva MR, Neto JM (2000) J Alloys Compd 313:168
4. Lopez N, Cid M, Puiggali M (1999) Corros Sci 41:1615
5. Pardal JM, Tavares, SSM, Cindra Fonseca, M, Souza JA, Vieira LM, Abreu HGF (2008) Caracterizaçâo microscópica de fases deletérias precipitadas durante tratamentos isotérmicos em aço inoxidável superduplex. In: 18° Congresso Brasileiro de Engenharia e Ciências dos Materiais. Porto de Galinhas, PE, Brazil
6. Ramirez Londoño AJ (1997) Estudo da precipitação de nitreto de cromo e fase sigma por simulação térmica da zona afetada pelo calor na soldagem multipassse de aços inoxidáveis duplex. Dissertação de Mestrado, Universidade Estadual de São Paulo
7. Pardal JM, Tavares SSM, Cindra Fonseca M, Souza JA, Corte RRA, Abreu HGF (2009) Mater Charact 60:165
8. Image Tool version 3.0, University of Texas Health Science Center at San Antonio, free software
9. Cortie MB, Jackson EMLEM (1997) Metall Mater Trans A 28A:2477